Miner Petrol (2009) 97:129–138
DOI 10.1007/s00710-009-0087-9

ORIGINAL PAPER

On the breakdown of zircon upon "dry" thermal annealing

Tamás Váczi · Lutz Nasdala · Richard Wirth · Mathias Mehofer · Eugen Libowitzky · Tobias Häger

Received: 14 August 2008 / Accepted: 5 October 2009 / Published online: 17 October 2009

Abstract Zircon samples without and with secondary chemical alteration from diverse sources were subjected to heat treatment at 1400 °C for 96 h. Resulting new phases and textures suggest that decomposition of zircon into component oxides occurred in all experiments to various degrees. The crucible material was found to have a strong influence on the extent of breakdown, especially in the case of altered starting materials. In this study the progressive stages of the breakdown of zircon grains are described. The factors that may govern the decomposition are discussed, including radiation damage, secondary alteration and external reaction conditions (sample container, atmosphere). Alumina crucibles should generally be avoided in dry annealing of zircon, to minimise uncontrolled breakdown into oxides.

Editorial handling: A. Möller

T. Váczi (✉) · L. Nasdala · E. Libowitzky
Institut für Mineralogie und Kristallographie, Universität Wien,
Althanstraße 14,
1090 Wien, Austria
e-mail: tamas.vaczi@univie.ac.at

L. Nasdala
e-mail: lutz.nasdala@univie.ac.at

E. Libowitzky
e-mail: eugen.libowitzky@univie.ac.at

R. Wirth
Helmholtz-Zentrum Potsdam, Deutsches GeoForschungsZentrum,
Telegrafenberg,
14473 Potsdam, Germany
e-mail: wirth@gfz-potsdam.de

M. Mehofer
Vienna Institute for Archaeological Science (VIAS),
Universität Wien,
Franz Klein-Gasse 1,
1190 Wien, Austria
e-mail: mathias.mehofer@univie.ac.at

T. Häger
Institut für Geowissenschaften,
Johannes Gutenberg-Universität Mainz,
Saarstr. 21,
55099 Mainz, Germany
e-mail: tobias.haeger@uni-mainz.de

Introduction

Zircon, $ZrSiO_4$, is a common accessory mineral found in a wide range of igneous and metamorphic rocks. It is the most important mineral for U/Th–Pb geochronology because (i) zircon is an extremely robust container for parent U and Th and daughter isotopes through geologic time and (ii) this mineral mostly excludes Pb at primary growth. For industrial purposes, zircon is a widely used refractory material for high-temperature applications such as furnace linings, barrier coatings, ceramic pigments etc. In addition, zircon is the primary source for zirconium and zirconia (ZrO_2).

Natural zircon has generally a non-ideal structure and composition, and industrial zircon is often processed, perhaps purified, natural zircon (see e.g. Pavlik et al. 2001). Depending on age, thermal history and actinide concentration, natural zircon has a certain level of accumulated radiation damage. The expected high-temperature behaviour of radiation-damaged (but not fully amorphised) zircon is a gradual restoration of short and long-range order (e.g. McLaren et al. 1994; Colombo and Chrosch 1998; Colombo et al. 1999; Begg et al. 2000; Capitani et al. 2000; Zhang et al. 2000; Nasdala et al. 2001; Geisler 2002; Nasdala et al. 2004). In contrast, the structural reconstitution of fully metamict zircon upon dry heating involves an

intermediate stage of ZrO_2 formation between 800 and 1100 °C, prior to the formation of crystalline zircon at above ca. 1150 °C (Mitsuhashi et al. 1974; Ellsworth et al. 1994; Zhang et al. 2000; Nasdala et al. 2002).

Pure, undamaged zircon is predicted to be stable up to ca. 1676 °C (e.g. Butterman and Foster 1967), at which point it decomposes into oxides. However, it is far from uncommon to observe that zircon breaks down at temperatures well below the thermodynamically predicted decomposition temperature. There appears to be no well-defined temperature for the onset of decomposition. Peña and de Aza (1984) and Kaiser et al. (2008) compiled zircon decomposition temperatures from the literature, ranging from 1400 °C to 2000 °C, but cited reports of incongruent melting at higher temperatures as well.

High-temperature treatment of zircon is done for various reasons in radioactive dating methods as well. The zircon whole-grain evaporation method (Kober 1986, 1987) utilises the decomposition of zircon into oxides (ZrO_2 + SiO_2) at elevated temperatures, where Pb is removed from zircon through the volatilisation of the silica component. Zircon evaporation is carried out on grains wrapped in inert rhenium filaments under vacuum (at ca. 1400–1500 °C). The "chemical abrasion" technique (multi-step leaching and thermal ionisation mass spectroscopy of whole zircon grains, CA-TIMS; Mattinson 2005) involves thermal preconditioning, prior to multi-step partial dissolution analysis, in order to partially stabilise radiation-damaged domains for a better-controlled etching behaviour. For this, Mattinson (2005) suggested to do heat treatment in air in alumina crucibles, at 800–1100 °C for 48 h. Note, however, that most geochronology laboratories seem to use SiO_2 crucibles instead of alumina.

This paper presents results of annealing experiments aimed to observe the progress of the breakdown of zircon. In our study the temperature for heat treatment was chosen at 1400 °C. This temperature is within the reported range of decomposition temperatures, high enough to anneal radiation damage (not studied here), yet significantly below the thermodynamically expected decomposition temperature of zircon. We attempt to evaluate factors influencing the decomposition behaviour of zircon, with special attention to chemical alteration of radiation-damaged domains. The role of thermal breakdown in age determination methods involving high-temperature treatment is discussed.

Materials and methods

Table 1 gives a summary of materials and experiments in this study. Three types of samples were included. First, we studied pure (undoped), synthetic zircon single crystals (1–2 mm), grown using the Li–Mo flux method (Hanchar et al. 2001). Second, fragments (0.5–2 mm) of well-characterised, inclusion-free zircon crystals were also studied, including the 1064 Ma old sample 91500 from Ontario, Canada (Wiedenbeck et al. 2004), and the late Precambrian–Cambrian gemstones M257, M127 (Nasdala et al. 2008), M146 and M144 (Nasdala et al. 2004) from Sri Lanka. In addition, zircon grains (sample 87165; Pérez-Soba et al. 2007) from a coarse-grained leucogranite of the Hercynian La Pedriza pluton, Spanish Central System batholith, were also studied. This zircon was heavily altered by secondary hydrothermal processes, and consequently it is chemically impure, significantly hydrated and has a large number of pores and mineral inclusions (Nasdala et al. 2009).

Small (0.5–1 mm) euhedral grains or chips of larger crystals were heated in either platinum or sintered Al_2O_3 crucibles. The crucibles were covered with a lid of the same material and placed in a larger alumina crucible to further reduce the exchange of gaseous species between crucible and furnace atmosphere. The samples were heated at 1400 °C in high-temperature furnaces for 96 h. The heating rate was typically ca. 50 °C/min (fast heat-up). The furnaces were equipped with type B thermocouples, temperature was regulated by the built-in controllers, the temperature accuracy was better than 50 °C. After 96 h the furnaces were switched off. Samples were removed only after the furnaces had cooled to room temperature. An attempt was made to check the effect of the rate of heat-up: a set of unaltered samples (Table 1) was subjected to annealing with a very flat ramp (1 °C/min) in a Pt crucible.

Following heat treatment, outer surfaces of the samples were imaged on uncut grains. Some grains were then embedded in araldite epoxy, ground to approximately half thickness and polished to reveal internal textures for scanning electron microscope (SEM) imaging. For transmission electron microscopy (TEM) analyses, electron transparent foils were prepared with the focused ion beam (FIB) technique (Wirth 2004).

Secondary electron (SE) and back-scattered electron (BSE) images of unprepared grains (i.e., no polishing and carbon coating) were taken in a LEO EVO 60 variable-pressure SEM, used in the low-vacuum mode. Epoxy-mounted samples were carbon coated and imaged using a JEOL JSM-6400 SEM. Sub-micrometer textures and compositions on FIB foils were studied with an FEI Tecnai G^2 F20 X-Twin analytical TEM operated at 200 kV in selected area electron diffraction (SAED), high-resolution (HRTEM) and scanning TEM (STEM) modes. For phase identification TEM and Raman spectroscopy were used. Raman spectra were acquired with a Renishaw RM1000 system in the quasi-confocal mode. The instrument was equipped with a Leica DMLM optical microscope, edge filter-based laser line rejection, an optical grating (1200

Table 1 Summary of sample materials and heat-treatment experiments

Zircon sample			Alpha dose[a]	References	Crucible material[b]	
Name	Origin	Character			50 °C/min	1 °C/min
syn		synthetic	0	Hanchar et al. (2001)	Pt, Al_2O_3	–
91500	Ontario, Canada	unaltered	0.33	Wiedenbeck et al. (2004)	Pt, Al_2O_3	Pt
M144	Sri Lanka	unaltered	0.88	Nasdala et al. (2004)	Pt, Al_2O_3	Pt
M257	Sri Lanka	unaltered	1.71	Nasdala et al. (2008)	Pt, Al_2O_3	Pt
M127	Sri Lanka	unaltered	1.83	Nasdala et al. (2008)	Pt, Al_2O_3	Pt
M146	Sri Lanka	unaltered	1.98	Nasdala et al. (2004)	Pt, Al_2O_3	Pt
87165	La Pedriza, Spain	altered	7–17	Pérez-Soba et al. (2007); Nasdala et al. (2009)	Pt, Al_2O_3	–

[a] Calculated doses, given in 10^{18} alpha events per gram. Values were extracted from the references quoted

[b] Materials: Pt—platinum, Al_2O_3—sintered alumina

grooves/mm), and a Si-based, Peltier-cooled CCD detector. The 632.8 nm emission of a He-Ne laser was used as the excitation source, and the elastic (Rayleigh) scattering was used for spectral calibration. The spectral resolution of the system was ca. 2.2 cm^{-1}; the wavenumber accuracy was better than 1 cm^{-1}. Modal composition and pore space estimates were obtained from BSE images using the ImageJ image processing and analysis program (available at http://rsbweb.nih.gov/ij/). The method is based on the assumption that the volume fractions of different phases or pore space are represented by the relative two-dimensional surface areas of greyscale shades measured on cross-sections.

Results

All samples display, though to largely varying degrees, evidence of reactions after the heat treatment, partly on outer surfaces and partly also internally. Zirconium oxide as a reaction product has been observed in all samples after heat treatment. The monoclinic polytype (baddeleyite) has been identified at room temperature using Raman spectroscopy (Fig. 1) and TEM (electron diffraction and chemical analysis). Zirconia shows pronounced polysynthetic twinning (Fig. 2b), suggesting a transformation from a higher-symmetry polymorph upon cooling. Tetragonal ZrO_2 has not been observed.

Silica has been found in the amorphous state, suggested by a diffuse ring in the TEM SAED patterns. TEM chemical point analysis reveals that silica contains impurity elements (Mg, Ca, Al, P) in the percent range. SiO_2 is positively identified only in sample 87165, in Pt-annealed grains and in internal zones of alumina-annealed grains where a zircon matrix is found after heat treatment (Fig. 2a, c). A thin layer of an unidentified transparent material, seen as coloured interference fringes on a reflected-light optical microscope image, is observed in some reaction pits (e.g. on M257). Raman spectra recorded from these thin layers lack characteristic bands of any known SiO_2 polymorph, but show a very high luminescence background (and peaks from underlying zircon). The thickness of these layers is estimated from the interference colours (assuming refractive index $n = 1.5$) to be less than 0.5 µm.

No strong evidence for the presence of silica is found in most of the reaction pits on the surfaces or in zirconia

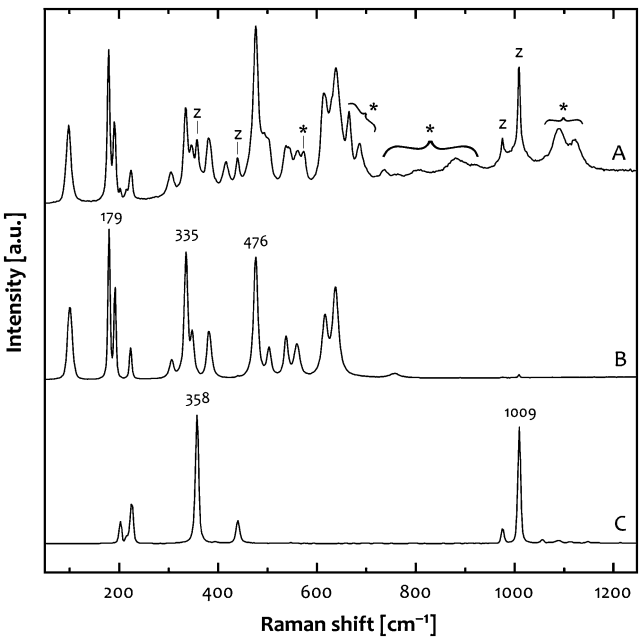

Fig. 1 Representative Raman spectra of decomposition products. **a** Typical spectrum recorded from a baddeleyite (monoclinic ZrO_2) microcrystal on the surface of an annealed grain (as in Fig. 3b). Underlying bulk zircon (bands labelled with "z") is also detected because of the moderate depth resolution of the Raman system used. Asterisks mark rare-earth luminescence artefacts from baddeleyite. Sample M257, fast heating, Al_2O_3 crucible. **b** Spectrum of pure baddeleyite from a porous crust (as in Fig. 3c). Synthetic sample, fast heating, Al_2O_3 crucible. (**c**) Zircon spectrum. Sample 91500, slow heating, Pt crucible (cf. Fig. 5b)

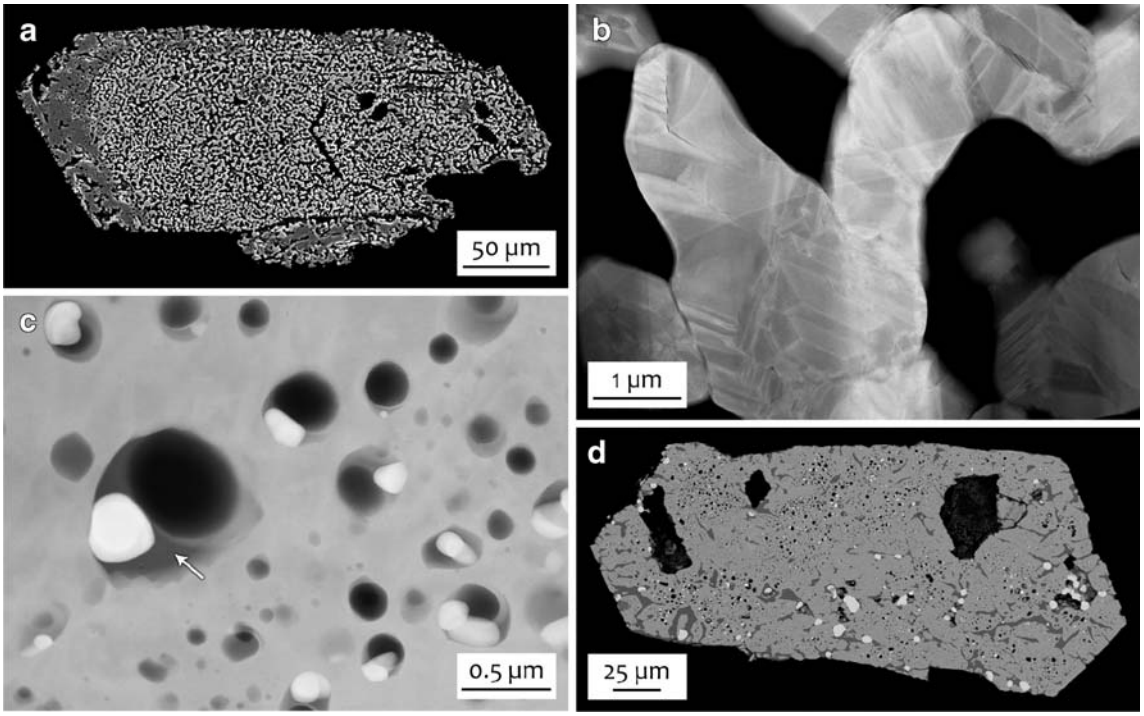

Fig. 2 The heavily altered La Pedriza zircon (sample 87165) after annealing. **a** Cross-section (SE image) of a grain annealed in an alumina crucible. The majority of the grain turned into a porous network of monoclinic zirconia (baddeleyite) while the silica component evaporated. The outer shape retains that of primary zircon. Note the recrystallised zircon zone, showing up in a darker tone on the left. **b** STEM image of a part of the zirconia network, cut out with FIB from the grain in (A). The lamellar fine contrast shows polysynthetic twinning. **c** STEM image of a FIB foil cut from the zircon rim of the grain in (A). White grains are baddeleyite, light grey areas are zircon. The arrow points to impure, amorphous silica. **d** BSE image of another grain, annealed in a Pt crucible. White dots are baddeleyite, mid-grey is zircon and dark grey patches are silica. The larger, angular, black areas are empty spaces left after inclusions (xenotime)

aggregates of heat-treated synthetic and unaltered samples (Figs. 3 and 4). Significant amounts of silica are "missing" from reaction zones that were in close contact with alumina crucibles. However, no reaction phase could be identified with Raman spectroscopy on the inner surface of the alumina crucibles at the sites of contact with the grains.

Decomposition textures have been observed either confined to outer surfaces or scattered throughout the volume of the grain. Surface breakdown has occurred in synthetic $ZrSiO_4$ and natural, unaltered zircon samples (syn, M127, M257, M144, M146 and 91500), while the hydrothermally altered La Pedriza zircon (sample 87165) exhibits oxide phases in the interior of the grains as well.

Synthetic $ZrSiO_4$ and unaltered zircon grains show only minor breakdown after being heated slowly (i.e., at ca. 50 °C/min) in Pt crucibles. The synthetic $ZrSiO_4$ sample

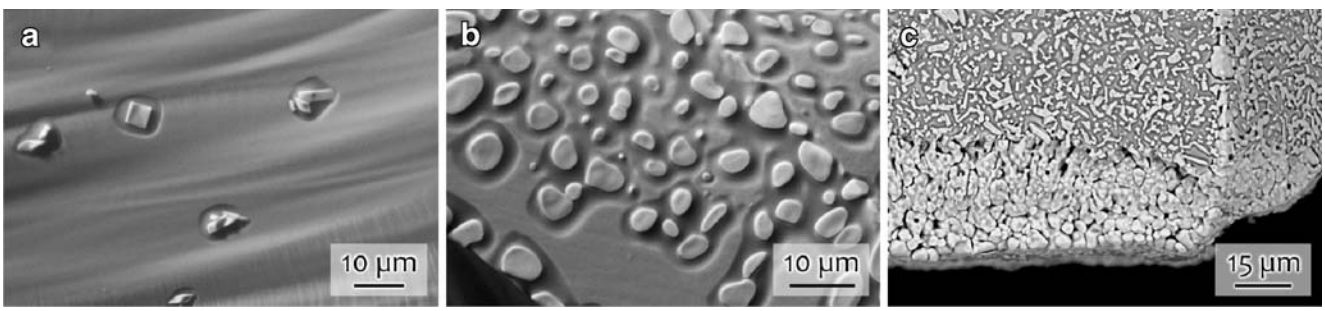

Fig. 3 Images showing the advance of surface corrosion of unaltered zircon (fast heating, alumina crucible). **a** Initial stage. Small pits (less than 0.5 µm deep) develop where zirconia crystals grow. Sample M127, SE image. **b** Intermediate stage. The pits fuse but zirconia crystals are still isolated. Sample M257, SE image. **c** Advanced stage. The breakdown reaction proceeds towards the inside of the zircon grain. Silica has evaporated and an aggregated zirconia rim develops. The bottom face of the crystal was in contact with the alumina crucible (see also Fig. 4). Synthetic $ZrSiO_4$ sample, BSE image

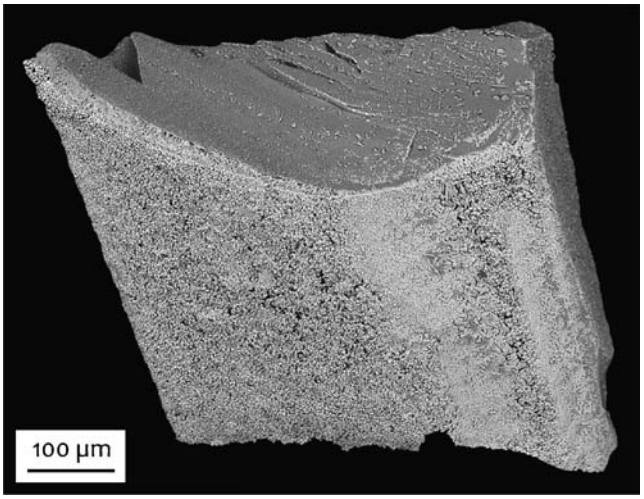

Fig. 4 BSE image of the M146 zircon gem fragment annealed in an alumina crucible. The side facing the page was in contact with the crucible and developed a porous baddeleyite crust. Note the highly accelerated breakdown (up to 30 µm away from the surface) on this side, while other sides of the grain display only point corrosion

displays a great number of very small (<2 µm) reaction pits, whereas the natural grains have very few, slightly larger (up to 10 µm), isolated reaction pits on the grain surfaces. Somewhat different textures have developed after slow heating (ca. 1 °C/min) of the unaltered samples in a Pt crucible. There is again only minor breakdown, and all of the annealed fragments show zirconia grains that lie near the grain surfaces. However, some of these zirconia crystals are found underneath a thin (<5 µm) layer of zircon, while the rest sit recessed into the surface (Fig. 5a–b; compare Fig. 3a–b). No perceptible difference between bulk zircon and the thin cover layer was detected on SEM images (BSE brightness, texture). No trace of silica is observed on polished cross-cuts (Fig. 5b).

Synthetic $ZrSiO_4$ and unaltered zircon samples annealed in alumina crucibles (fast heat-up) decompose more extensively, as shown in Fig. 3a–c. A peculiar feature is that a zirconia aggregate crust develops only on one side of the grain, namely on the side of the fragment, or face of the crystal, that was in physical contact with the crucible during annealing. After heating for 96 h, the reaction front (zircon–porous zirconia interface) has advanced 10–30 µm inwards from the original surface (Figs. 3c and 4). Note that on the same grains the faces that have not been in contact with alumina are sparsely covered with reaction pits and isolated zirconia grains.

From the observed abundance and extent of the breakdown that develops on outer surfaces (synthetic $ZrSiO_4$ and unaltered samples), the progressive stages of the process may be reconstructed. The decomposition of synthetic $ZrSiO_4$ and unaltered zircon during annealing usually starts at the outer surface and proceeds inwards (Figs. 3 and 4). The process starts with isolated, shallow pits on the surface, with a flat zirconia grain in the centre (Fig. 3a). As the decomposition proceeds, the pits grow laterally but not significantly in depth (Fig. 3b). The pits eventually merge and cover the entire surface, but the zirconia grains remain isolated. The further breakdown of zircon then advances away from the surface, and the zirconia grains are eventually sintered into a porous aggregate (Fig. 3c) when a zircon substrate supports them no longer. At this stage the reaction front proceeds inwards, roughly parallel to the surface, leaving a sponge-like zirconia network with very little or no silica. The breakdown may advance so far that the entire zircon material is consumed. The leftover zirconia aggregate retains the outer shape of the original zircon grain.

In annealed grains of sample 87165, the breakdown products are not limited to the surfaces. The zircon grains annealed (fast heat-up) in an alumina crucible show the

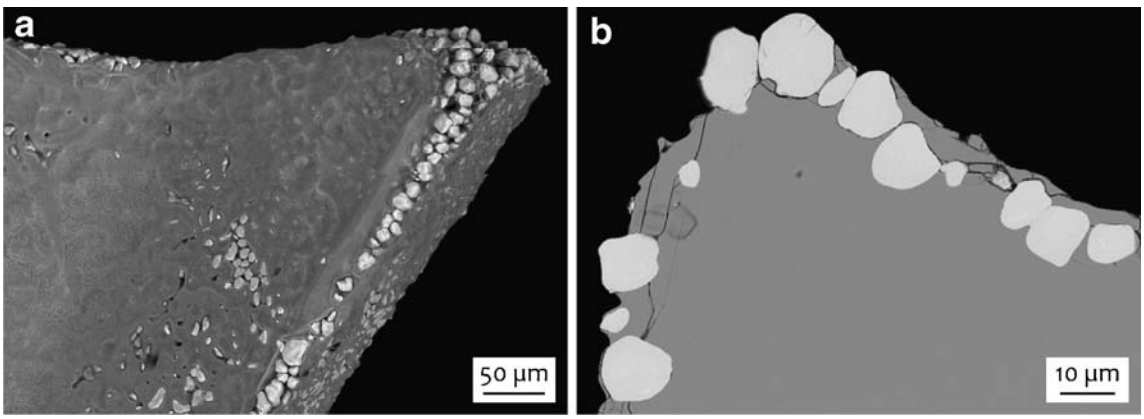

Fig. 5 Images of an annealed grain of sample 91500, after slow heating (1 °C/min) in a Pt crucible. **a** BSE image of the unprepared grain. The zirconia crystallites are partly embedded in the zircon and appear mostly at the edges. The zircon surface shows mottled contrast but no corrosion pits are seen, unlike in Fig. 3. **b** BSE image of a polished section of the grain in (A). Zirconia crystals (bright, rounded grains) are located somewhat below the zircon surface. There is no BSE intensity difference between bulk and cover zircon. Note that there is no visible trace of silica, and pore space is negligible

most extensive breakdown: 80–100 vol% of each grain consists of a sponge-like, porous network of monoclinic zirconia (Fig. 2a–b) without observable traces of silica. The volume ratio of zirconia to pore space is estimated to be close to 50:50, with ±5% error. In some, but not all, grains there are areas of irregular shape where zircon is observed after heat treatment (Fig. 2a). Electron diffraction patterns made on FIB foils cut from such zircon zones reveal polycrystalline zircon. The crystallites are not oriented, suggesting recrystallisation without major directional control by epitaxial growth. There are tiny (0.1–2 μm), round inclusions, scattered irregularly in the zircon matrix. The inclusions are filled with amorphous silica that covers the walls and hosts a rounded ZrO_2 grain. The centre of the inclusions is pore space (Fig. 2c).

Grains of sample 87165 annealed in a Pt crucible (fast heat-up) show a different internal texture. The formation of polycrystalline zircon is much more pronounced and coexisting silica glass and zirconia are also observed after the heat treatment (Fig. 2d). Zircon was identified in ca. 75–90% of the grain volume; the rest of the grains is made up of amorphous silica (8–17%), monoclinic zirconia (2–4%) and pore space (2–5%; Fig. 2d). (Note that these numbers are rough estimates, as the method used to derive them is strongly influenced by the resolution, the contrast and the noise of BSE images. Values for zirconia, silica and pore space may especially have large errors either due to small grain size or small differences in their greyscale levels.) Rounded silica–zirconia–pore inclusions (identical to those found in samples annealed in an alumina crucible, cf. Fig. 2c) are abundant.

Discussion

In the phase diagram of the ZrO_2–SiO_2 system published by Butterman and Foster (1967), pure $ZrSiO_4$ was predicted to be stable up to 1676±7 °C. Kamaev et al. (2005) refined the same stability limit at 1674±7 °C. O'Neill (2006) predicted 1665 °C based on thermodynamical calculations. Most recently, Kaiser et al. (2008) arrived at the value of 1673±10 °C. However, zircon decomposition at the above temperatures seems to be the exception rather than the rule. In this study, decomposition was observed at 1400 °C, Kober (1986) observed breakdown between 1380 and 1480 °C, Mursic et al. (1992) reported a temperature of 1477 °C, Pavlik et al. (2001) recorded 1285 °C, Wang et al. (2006) and Wanthanachaisaeng et al. (2006) saw reaction products after heat treatment at 1400 °C, while Davis (2007) inferred a phase separation below 1550 °C. (See also Peña and de Aza 1984 and Kaiser et al. 2008 for a list of other temperature data.) The appearance of zirconia was observed even at unusually low temperatures by Zhang et al. (2000: 852 °C) Capitani et al. (2000: 927 °C) and Nasdala et al. (2002: between 800 and 950 °C) in fully metamict starting materials.

Effects of radiation damage

The synthetic and unaltered samples used in this study span an initial range in radiation damage from zero (syn) to moderate (M146; see Table 1). The character and the extent of breakdown observed on these samples suggest that initial radiation damage up to moderate levels has little influence on thermal decomposition. This is in agreement with Chapman and Roddick (1994), who found that appreciably different U concentrations and self-irradiation levels (10 ppm U, 1334 Ma vs. 160 ppm U, 2680 Ma; very low to moderate radiation damage) had little or no effect on the rate of zircon decomposition in vacuum.

Moderate radiation damage means that amorphous damage clusters are isolated in a defect-rich crystalline matrix. At high temperatures, a "self-epitaxial" recrystallisation of the damaged volumes, besides point defect annealing, is expected to occur (see Ewing et al. 2003). In contrast, in completely metamict zircon essentially the entire volume is amorphous. Monaghan et al. (2005) stated that amorphous SiO_2–ZrO_2 mixtures are thermodynamically unstable with respect to a mixture of solid oxides. Calculations by Kim and McIntyre (2002) also show that amorphous ZrO_2–SiO_2 mixtures with composition between 40–90 mol% SiO_2 should decompose into amorphous silica-rich and zirconia-rich phases at temperatures as low as 600 °C. Lucovsky and Rayner (2000) observed demixing of vapour-deposited Zr silicate films between 800 and 900 °C. Carrez et al. (2003) arrived at similar conclusions, i.e. at low temperatures amorphous $ZrSiO_4$ should undergo spinoidal decomposition as the component oxides are in the immiscibility domain.

Thus, spontaneous disintegration into a mixture of oxides in the amorphous volume is expected to occur prior to recrystallisation of fully metamict zircon upon heating. The appearance of zirconia in heavily damaged primary (unaltered) zircon at very low temperatures (Zhang et al. 2000; Capitani et al. 2000 and Nasdala et al. 2002; see above) is therefore not due to a decomposition reaction but results from the demixing of amorphous (metamict) zircon into more stable oxides.

Effects of alteration

The chemical resistance of heavily damaged zircon is significantly decreased against dissolution (e.g. Lumpkin 2001). A reaction of damaged zircon with fluids often yields secondary zircon in which the original texture, major and minor element composition and isotope concentrations

are modified (e.g. Geisler et al. 2002; Geisler et al. 2003a). Secondary, altered zircon, such as sample 87165, is generally porous with micrometre to nanometre-scale pores (Putnis 2002; Nasdala et al. 2009), enriched in non-formula elements (especially, P, Fe, Ca, Al etc.; e.g. Geisler et al. 2003b), mineral inclusions (e.g. xenotime) and hydrous species (Nasdala et al. 2009).

The high-temperature behaviour of strongly altered zircon (sample 87165) is poorly understood but alteration apparently has a profound influence on decomposition (Fig. 2). The effects of porosity, non-formula elements, mineral inclusions and hydrous content (Nasdala et al. 2009) are impossible to separate from each other. Enhanced porosity offers abundant pathways for element mobility in contrast to dense zircon. The "colourful" chemistry (non-formula elements in the percent range) is inferred to play a role in lowering temperatures of dissociation reactions and, along with solid (mineral) inclusions, has a strong influence on phase equilibria (see e.g. Peña and de Aza 1984). The hydrous species, apart from lowering reaction temperatures, may react with silica and may chemically bind to or volatilise available SiO_2. In general, SiO_2 appears to be significantly more mobile in altered than in unaltered zircon, as seen from the nearly complete reaction of silica with the alumina crucible (Fig. 2a). At the same time, the reassociation of silica with zirconia is apparently limited, suggested by the coexistence of the two phases after four days of annealing (Fig. 2c–d). Experimental results presented in this paper do not allow us to draw precise conclusions about the effect of alteration on the thermal behaviour of zircon.

Effect of reaction conditions

The decomposition in synthetic $ZrSiO_4$ and unaltered samples is always related to outer surfaces, implying that the reaction is initiated by external influences, i.e. effects not related to bulk zircon properties. However, we have no direct explanation as to what actually starts the point corrosion, which then extends first into pits and then a breakdown front proceeding inwards.

The differences in the extent of breakdown between Pt and Al_2O_3 crucibles are attributed to the crucible material. Generally, surface corrosion (synthetic and unaltered samples) is more advanced in alumina-annealed grains (Figs. 2a, 3c and 4) compared to Pt-annealed analogues. The effect of alumina is most pronounced on the grain surfaces that were in physical contact with the alumina crucible: in these areas the breakdown reaction reached a clearly more advanced stage (Figs. 3c and 4). The same is observed on grains of sample 87165 (altered zircon), where free silica is seen after annealing in a Pt crucible, whereas very extensive silica removal is observed in alumina crucibles.

We assume that the silica reacted with alumina and the equilibrium shifted in favour of further decomposition. According to Zhao et al. (2003), a reaction between amorphous silica (a liquid state was suggested by Peña and de Aza 1984) and Al_2O_3, forming an aluminosilicate glass, occurs already below 1350 °C. However, without crystalline mullite seeds, mullite nucleates from an amorphous state only above 1400 °C (Zhao et al. 2003), which may well explain why no third phase was identified using Raman spectroscopy in alumina crucibles.

Similar conclusions can be drawn for the zircon inclusions in heat-treated ruby (Wang et al. 2006; Wanthanachaisaeng et al. 2006). In a zircon inclusion decomposition should not be observed if the host mineral is inert with respect to the breakdown products. This is not the case with corundum, and thus ZrO_2 is formed because the reaction between SiO_2 and Al_2O_3 forms an aluminosilicate phase, preventing the recrystallisation of zircon.

Our results seem to indicate that zircon is chemically less resistant than it is often assumed. Direct contact of zircon with a potentially reactive material should therefore be avoided during the high-temperature treatment of zircon gems. Also, for long-term nuclear waste storage purposes care should be taken to avoid contact between zircon as waste form and any container material that may react with silica.

A comparison of our results to other studies in the literature reveals that the reaction atmosphere also has an influence on the breakdown of zircon into component oxides well below the thermodynamic decomposition temperature. The products of the breakdown reaction (especially ZrO_2) have been observed when annealing in air (e.g. under atmospheric pressure in this study), under vacuum (e.g. Kober 1986; 1987; Ansdell and Kyser 1993; Chapman and Roddick 1994), in a hot combustion atmosphere (Fritsch et al. 2006) and in a reducing, gaseous atmosphere (Gardner and Buchanan 1975; Barreiro et al. 2009) as well.

The reaction atmosphere appears to influence the activity of silica in the vicinity of the grain surfaces. We assume that the flow of volatile species away from the grain surface, following the concentration/pressure gradient, is the main driving force under vacuum. In a hot combustion atmosphere (significant H_2O partial pressure), such as that found in gas turbine engines, Fritsch et al. (2006) suggested the reaction of SiO_2 with water vapour forming volatile $Si(OH)_4$. In a reducing atmosphere, Gardner and Buchanan (1975) suggested a direct volatilisation of SiO_2 and its reduction into SiO by H_2 or CO. In low-pressure experiments (10^{-3} atm) done in a graphite furnace, Barreiro et al. (2009) reported that an increasing partial pressure of O_2 (2×10^{-9}–2×10^{-4} atm) in the furnace resulted in an increase in the weight loss of heated zircon samples. They explained this trend by suggesting a reaction between the graphite

furnace and oxygen to form CO, which then reduces SiO_2 into volatile SiO. Pavlik et al. (2001) used mass spectroscopy to identify volatile SiO during vacuum heating of zircon, i.e. without a reducing atmosphere.

The zircon samples heated in reducing (Gardner and Buchanan 1975; Barreiro et al. 2009) and hot combustion atmospheres (Fritsch et al. 2006) develop porous zirconia crusts analogous to zircon heated in air (Figs. 3c and 4) or in vacuum (Ansdell and Kyser 1993; Chapman and Roddick 1994). We find it questionable that reducing agents (CO, H_2) or water vapour actually reach the zircon–baddeleyite reaction front once it is covered by a porous zirconia crust. We instead think that a volatilisation of SiO_2 occurs at or near the reaction front, SiO_2(g) diffuses through porous zirconia into the furnace atmosphere and reduction (to SiO) or hydroxide formation ($Si(OH)_4$) may occur only there, accelerating the reaction by decreasing the amount (partial pressure) of SiO_2 available. The decomposition of zircon therefore is not caused, only indirectly enhanced, by reductive gases or water vapour. Gas flow, as in the experiments of Fritsch et al. (2006), further increases the removal of volatile species.

Air is essentially free of reducing gases (given that no reduction occurs in the heated furnace) and the concentration of water vapour is typically very low (<22.9 $g\,m^{-3}$ at 25 °C, which becomes <4.1 $g\,m^{-3}$ when heated to 1400 °C). We expect that if no reaction occurs between evaporated silica and the reaction atmosphere (N_2, O_2, CO_2) and crucible material (e.g. Pt), the reaction rate will be lower in dry-air annealing compared to heat treatment in reductive or hydrous atmospheres. Furthermore, air pressure may also decrease the rate at which SiO_2(g) diffuses away from the reaction environment, therefore we expect the advance of the zircon–baddeleyite reaction front to be slower in a non-reducing gas atmosphere than in vacuum.

Implications for age determination techniques

We propose that thermal decomposition of zircon plays a key role in the success of age determination techniques that employ heat treatment. Two techniques are briefly outlined and the role of thermal decomposition is explained below.

In the whole-grain zircon evaporation technique of Kober (1986, 1987) and related methods (Davis 2007) a zircon grain is wrapped in a strip of rhenium foil (evaporation filament) so that only a thin slit is open facing a second Re filament (ionisation filament). Heating the zircon grain up to ca. 1230 °C is found to remove lead loosely bound (adsorbed) on surfaces and from highly leached (altered) domains. After such preconditioning, successively higher-temperature evaporation steps between 1330–1530 °C are used to decompose and evaporate zircon domains with decreasing Pb loss (for more details see Kober 1987 and Ansdell and Kyser 1993). In the CA–TIMS technique (Mattinson 2005), thermal preconditioning of whole zircon grains is done at 800–1100 °C in air for 48 h. After heat treatment the U/Th–Pb system is analysed through stepwise dissolution and mass spectroscopy (partial dissolution analysis, PDA). The key to the success of PDA is the heat treatment; without annealing PDA is not so effective.

A common feature in the two techniques is that there is an evolution of the isotope ratios in progressive evaporation/dissolution steps from open-system ("discordant") towards closed-system ("concordant") character. Note that Kober (1986; 1987) and Ansdell and Kyser (1993) associated the later stages (i.e., higher temperatures) of breakdown with increasing crystallinity. The results in this study (compare Figs. 3c and 4) and those of Chapman and Roddick (1994) suggest that structural damage up to moderate levels is not a major factor that governs the decomposition reaction. We need to emphasize that structural damage due to self-irradiation does not directly induce Pb loss (or a change in composition in general), only diminishes the resistance of primary zircon against dissolution (leaching).

Our results suggest that in zircon evaporation experiments the decomposition temperature of different domains is a function of the extent of chemical alteration. This is reflected in the order in which the zircon domains undergo breakdown: Pb will be released successively from domains less and less affected by Pb leaching and/or enrichment. The last domains to decompose will have a closed isotope system (no alteration), seen as a plateau $^{207}Pb/^{206}Pb$ age in TIMS.

We propose that in a CA–TIMS experiment different processes occur in zircon domains according to their alteration levels. Moderately damaged but unaltered domains experience a recovery of crystallinity. In altered or amorphous zones a phase separation into component oxides takes place. Partially decomposed zircon or a mixture of oxides is expected to be less stable, while the resistance of recrystallised zircon domains is increased against dissolution by HF. Subsequent PDA steps are therefore able to separate zircon zones according to the extent of breakdown developed during thermal preconditioning. Alumina crucibles (Mattinson 2005) may have the effect of reacting with silica, enhancing the decomposition of zircon. Note that the onset temperature of aluminosilicate glass formation in the reaction between zircon and alumina was put to ca. 1100 °C by Zhao et al. (2003), which is just at the upper limit of zircon annealing in the CA–TIMS technique. Annealing of zircon in SiO_2 crucibles, in contrast, may actually decrease the extent of breakdown by increasing silica activity in the reaction atmosphere. It appears worthwhile to test the two

crucible materials against each other in a chemical abrasion experiment.

Conclusions

The high-temperature breakdown of unaltered zircon below the generally accepted thermodynamical dissociation temperature (1665–1676 °C) is a surface corrosion process producing crystalline ZrO_2 and amorphous SiO_2. Silica is inferred to evaporate below 1400 °C. The extent of the breakdown is controlled by temperature and processes that decrease SiO_2 activity in the reaction environment, such as molecular flow or diffusion due to a concentration gradient, reaction of silica vapour with the atmosphere (e.g. reduction by H_2, CO or hydroxide formation with water vapour), solid-state reactions (e.g. with the crucible or the furnace material) or transport by a gas stream in the experimental chamber. Therefore if minimum decomposition is desired, a small-volume inert (e.g. Pt) crucible and a non-reactive atmosphere (such as N_2 or air) should be used to anneal zircon at high temperatures. Similar constraints may apply to containers designed to be used for nuclear waste storage.

Acknowledgements Samples studied in this research were kindly provided by J.M. Hanchar (synthetic zircon), M. Wiedenbeck (91500), W. Hofmeister (M127, M144, M146, M257), and C. Pérez-Soba (87165). Thanks are due to A. Wagner for the excellent sample preparation, and to B. Ullrich for obtaining a BSE image of an annealed La Pedriza zircon. We are grateful to I. Dódony and D.W. Davis for helpful discussions and suggestions. The constructive reviews by J.M. Hanchar and an anonymous expert, and detailed comments by associate editor A. Möller, greatly contributed to the manuscript. Partial funding for this study was provided by the European Commission through contract no. MEXC-CT-2005-024878 and by the Austrian Science Fund (FWF) through grant no. P20028-N10.

References

Ansdell KM, Kyser TK (1993) Textural and chemical changes undergone by zircon during the Pb-evaporation technique. Am Mineral 78:36–41

Barreiro P, Rey P, Souto A, Guitián F (2009) Porous stabilized zirconia coatings on zircon using volatility diagrams. J Eur Ceram Soc 29:653–659

Begg BD, Hess NJ, Weber WJ, Conradson SD, Schweiger MJ, Ewing RC (2000) XAS and XRD study of annealed ^{238}Pu— and ^{239}Pu-substituted zircons ($Zr_{0.92}Pu_{0.08}SiO_4$). J Nucl Mat 278:212–224

Butterman WC, Foster WR (1967) Zircon stability and the ZrO_2-SiO_2 phase diagram. Am Mineral 52:880–885

Capitani GC, Leroux H, Doukhan JC, Ríos S, Zhang M, Salje EKH (2000) A TEM investigation of natural metamict zircons: structure and recovery of amorphous domains. Phys Chem Minerals 27:545–556

Carrez P, Forterre C, Braga D, Leroux H (2003) Phase separation in metamict zircon under electron irradiation. Nucl Instrum Meth B 211:549–555

Chapman HJ, Roddick JC (1994) Kinetics of Pb release during the zircon evaporation technique. Earth Planet Sci Lett 121:601–611

Colombo M, Chrosch J (1998) Annealing of natural metamict zircons: II high degree of radiation damage. Radiat Phys Chem 53:563–566

Colombo M, Chrosch J, Salje EKH (1999) Annealing metamict zircon: a powder X-ray diffraction study of a highly defective phase. J Am Ceram Soc 82:2711–2716

Davis DW (2007) Sub-m.y. age resolution for Precambrian igneous events by thermal extraction (TE-TIMS) Pb dating of zircon: Application to progressive crystallization of the 1849 Ma Sudbury impact melt. Geochim Cosmochim Acta 71:A206

Ellsworth S, Navrotsky A, Ewing RC (1994) Energetics of radiation damage in natural zircon ($ZrSiO_4$). Phys Chem Minerals 21:140–149

Ewing RC, Meldrum A, Wang L, Weber WJ, Corrales LR (2003) Radiation effects in zircon. In: Hanchar JM, Hoskin PWO (eds) Zircon. Mineral. Soc. Am., Washington, D.C., pp 387–425

Fritsch M, Klemm H, Herrmann M, Schenk B (2006) Corrosion of selected ceramic materials in hot gas environment. J Eur Ceram Soc 26:3557–3565

Gardner RA, Buchanan RC (1975) High temperature loss of silica from zircon and refractory silicates. J Electrochem Soc 122:205–211

Geisler T (2002) Isothermal annealing of partially metamict zircon: evidence for a three-stage recovery process. Phys Chem Miner 29:420–429

Geisler T, Pidgeon RT, van Bronswijk W, Kurtz R (2002) Transport of uranium, thorium, and lead in metamict zircon under low-temperature hydrothermal conditions. Chem Geol 191:141–154

Geisler T, Pidgeon RT, Kurtz R, van Bronswijk W, Schleicher H (2003a) Experimental hydrothermal alteration of partially metamict zircon. Am Mineral 88:1496–1513

Geisler T, Rashwan AA, Rahn MKW, Poller U, Zwingmann H, Pidgeon RT, Schleicher H, Tomaschek F (2003b) Low-temperature hydrothermal alteration of natural metamict zircons from the Eastern Desert, Egypt. Mineral Mag 67:485–508

Hanchar JM, Finch RJ, Hoskin PWO, Watson EB, Cherniak DJ, Mariano AN (2001) Rare earth elements in synthetic zircon: Part 1. Synthesis, and rare earth element and phosphorus doping. Am Mineral 86:667–680

Kaiser A, Lobert M, Telle R (2008) Thermal stability of zircon ($ZrSiO_4$). J Eur Ceram Soc 28:2199–2211

Kamaev DN, Archugov SA, Mikhailov GG (2005) Study and thermodynamic analysis of the ZrO_2–SiO_2 system. Russ J Appl Chem 78:200–203

Kim H, McIntyre PC (2002) Spinodal decomposition in amorphous metal–silicate thin films: Phase diagram analysis and interface effects on kinetics. J Appl Phys 92:5094–5102

Kober B (1986) Whole-grain evaporation for ^{207}Pb/^{206}Pb-age-investigations on single zircons using a double-filament thermal ion source. Contrib Mineral Petrol 93:482–490

Kober B (1987) Single-zircon evaporation combined with Pb^+ emitter bedding for ^{207}Pb/^{206}Pb-age investigations using thermal ion mass spectrometry, and implications to zirconology. Contrib Mineral Petrol 96:63–71

Lucovsky G, Rayner GBJ (2000) Microscopic model for enhanced dielectric constants in low concentration SiO_2-rich noncrystalline Zr and Hf silicate alloys. Appl Phys Lett 77:2912–2914

Lumpkin GR (2001) Alpha-decay damage and aqueous durability of actinide host phases in natural systems. J Nucl Mater 289:136–166

Mattinson JM (2005) Zircon U–Pb chemical abrasion ("CA–TIMS") method: Combined annealing and multi-step partial dissolution analysis for improved precision and accuracy of zircon ages. Chem Geol 220:47–66

McLaren AC, Fitz Gerald JD, Williams IS (1994) The microstructure of zircon and its influence on the age determination from Pb/U isotopic ratios measured by ion microprobe. Geochim Cosmochim Acta 58:993–1005

Mitsuhashi T, Ichihara M, Tatsuke U (1974) Characterization and stabilization of metastable tetragonal ZrO_2. J Am Ceram Soc 57:97–101

Monaghan S, Greer JC, Elliott SD (2005) Thermal decomposition mechanisms of hafnium and zirconium silicates at the atomic scale. J Appl Phys 97:114911

Mursic Z, Vogt T, Frey F (1992) High-temperature neutron powder diffraction study of $ZrSiO_4$ up to 1900 K. Acta Crystallogr B 48:584–590

Nasdala L, Wenzel M, Vavra G, Irmer G, Wenzel T, Kober B (2001) Metamictisation of natural zircon: accumulation versus thermal annealing of radioactivity-induced damage. Contrib Mineral Petrol 141:125–144

Nasdala L, Lengauer CL, Hanchar JM, Kronz A, Wirth R, Blanc P, Kennedy AK, Seydoux-Guillaume A-M (2002) Annealing radiation damage and the recovery of cathodoluminescence. Chem Geol 191:121–140

Nasdala L, Reiners PW, Garver JI, Kennedy AK, Stern RA, Balan E, Wirth R (2004) Incomplete retention of radiation damage in zircon from Sri Lanka. Am Mineral 89:219–231

Nasdala L, Hofmeister WG, Norberg N, Mattinson JM, Corfu F, Dörr W, Kamo SL, Kennedy AK, Kronz A, Reiners PW, Frei D, Kosler J, Wan YS, Götze J, Häger T, Kröner A, Valley JW (2008) Zircon M257 — a homogeneous natural reference material for the ion microprobe U–Pb analysis of zircon. Geostand Geoanal Res 32:247–265

Nasdala L, Kronz A, Wirth R, Váczi T, Pérez-Soba C, Willner A, Kennedy AK (2009) The phenomenon of deficient electron microprobe totals in radiation-damaged and altered zircon. Geochim Cosmochim Acta 73:1637–1650

O'Neill HSC (2006) Free energy of formation of zircon and hafnon. Am Mineral 91:1134–1141

Pavlik RS, Holland HJ, Payzant EA (2001) Thermal decomposition of zircon refractories. J Am Ceram Soc 84:2930–2936

Peña P, de Aza S (1984) The zircon thermal behavior: effect of impurities. Part 1. J Mater Sci 19:135–142

Pérez-Soba C, Villaseca C, González del Tánago J, Nasdala L (2007) The composition of zircon in the peraluminous Hercynian granites of the Spanish Central System batholith. Can Mineral 45:509–527

Putnis A (2002) Mineral replacement reactions: from macroscopic observations to microscopic mechanisms. Mineral Mag 66:689–708

Wang WY, Scarratt K, Emmett JL, Breeding CM, Douthit TR (2006) The effects of heat treatment on zircon inclusions in Madagascar sapphires. Gems Gemol 42:134–150

Wanthanachaisaeng B, Häger T, Hofmeister W, Nasdala L (2006) Raman- und fluoreszenz-spektroskopische Eigenschaften von Zirkon-Einschlüssen in chrom-haltigen Korunden aus Ilakaka und deren Veränderung durch Hitzebehandlung. Z Dt Gemmol Ges 55:123–136

Wiedenbeck M, Hanchar JM, Peck WH, Sylvester P, Valley J, Whitehouse M, Kronz A, Morishita Y, Nasdala L, Fiebig J, Franchi I, Girard JP, Greenwood RC, Hinton R, Kita N, Mason PRD, Norman M, Ogasawara M, Piccoli PM, Rhede D, Satoh H, Schulz-Dobrick B, Skar O, Spicuzza MJ, Terada K, Tindle A, Togashi S, Vennemann T, Xie Q, Zheng YF (2004) Further characterisation of the 91500 zircon crystal. Geostand Geoanal Res 28:9–39

Wirth R (2004) Focused Ion Beam (FIB): A novel technology for advanced application of micro- and nanoanalysis in geosciences and applied mineralogy. Eur J Mineral 16:863–876

Zhang M, Salje EKH, Capitani GC, Leroux H, Clark AM, Schluter J, Ewing RC (2000) Annealing of α-decay damage in zircon: a Raman spectroscopic study. J Phys: Condens Mat 12:3131–3148

Zhao SK, Huang Y, Wang CA, Huang XX, Guo JK (2003) Mullite formation from reaction sintering of $ZrSiO_4/\alpha$-Al_2O_3 mixtures. Mater Lett 57:1716–1722